Part I
Results

1. Results for the fuel cell

First, a simulation for 8 individuals and 7 generations is performed. Fig 1 shows that the fitness of the best new values hardly changes. Only the fitness of the mean individuals improves on average.

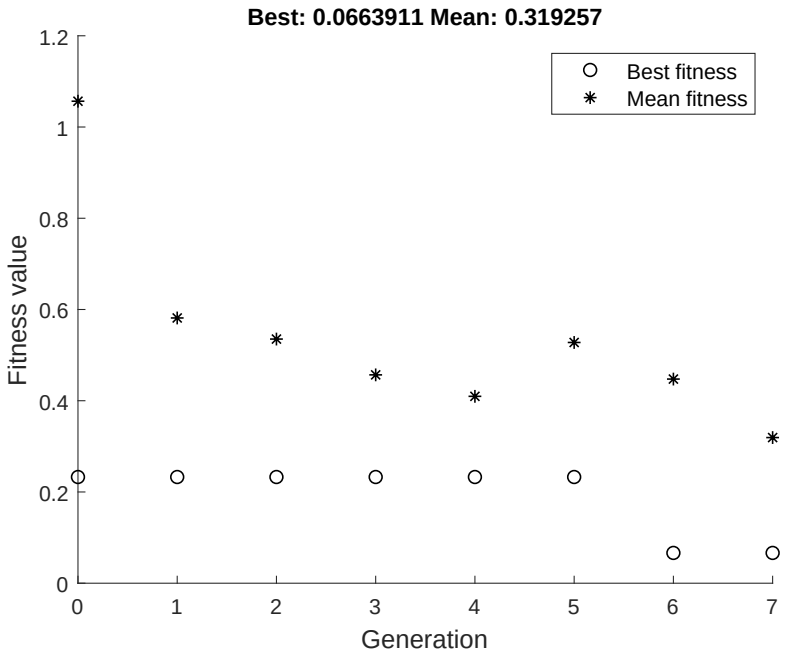

Figure 1: Development of fitness value for a population size of 8 individuals and after 7 generations

As the number of individuals increases, one sees in Fig. 2 that the fitness of the best as well as the bad individuals improves and the performance of average cell power density curve is barely different from the desired result.

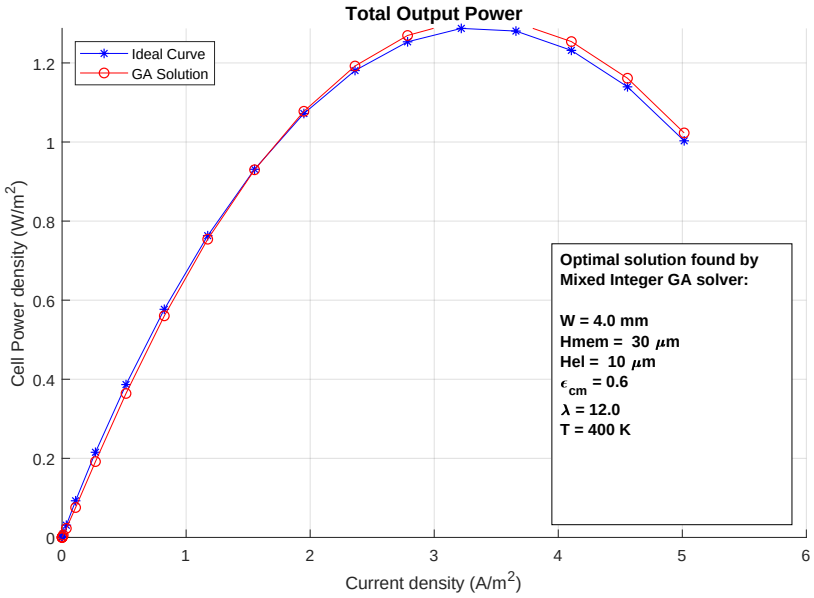

Figure 2: average cell power density curve

The following figure Fig.3 demonstrates the probabilistic nature of Genetic Algorithms which achieve approximately the same results when choosing different parameters. The solution is therefore not unique. In addition, that means that the desired parameters can be sought out.

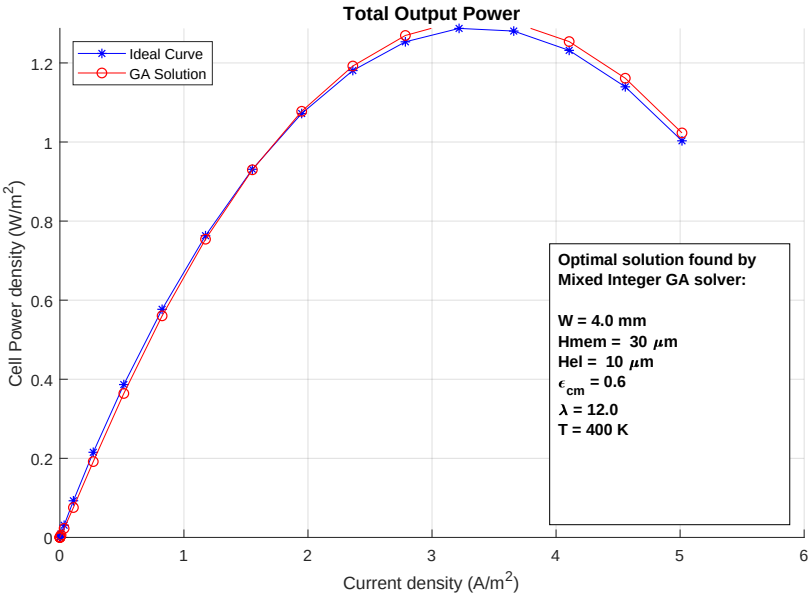

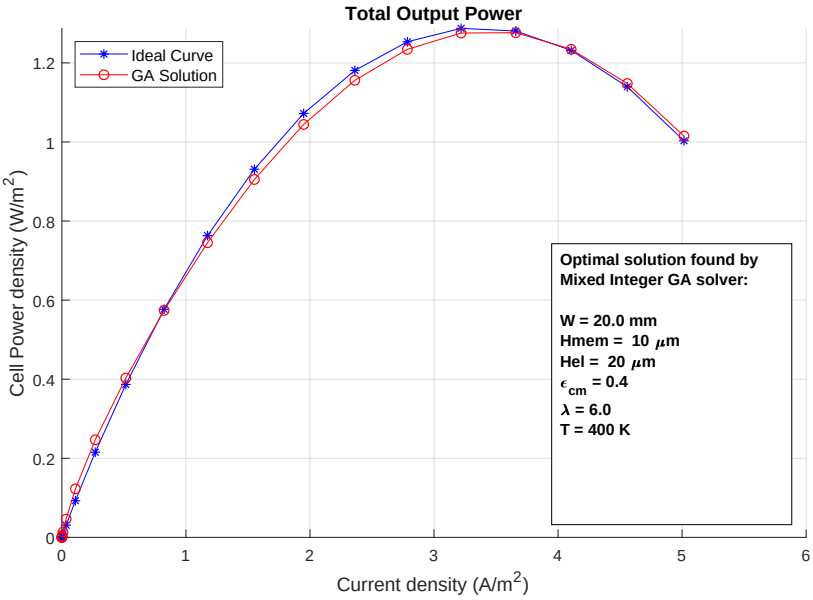

Figure 3: The plot shows the non uniqueness of the solution

2. Results for the reverberation chamber

2.1. Result of the optimized stirrer geometry

The objective function that we used is the Shapiro-Wilk-Test value P for the real and imaginary average electric field in each of the three directions in terms of the different parameters

$$F_P = \sqrt{\sum_{i=1}^{6} \left| P_i \left(tr_1y_1, tr_1y_2, tr_2y_1, tr_2y_2 \right) - 1 \right|^2} \rightarrow \min. \tag{1}$$

In order to use a genetic algorithm, a solution space must first be specified. In our case, the following parameters are listed in Table 1 where the range and step size that are necessary for the resolution of the solution space. These values change the shape of the wings.

Table 1: Solution space for genetic algorithms

Symbol	Range	Step size	Unit	Description
tr_1y_1	$\begin{bmatrix} 240 & 330 \end{bmatrix}$	9	mm	distance
tr_1y_2	$\begin{bmatrix} 240 & 330 \end{bmatrix}$	9	mm	distance
tr_2y_1	$\begin{bmatrix} 10 & 100 \end{bmatrix}$	9	mm	distance
tr_2y_2	$\begin{bmatrix} 10 & 100 \end{bmatrix}$	9	mm	distance

From the solution space, as shown in Table 1, an initial population is randomly generated. The algorithm improves this population during the simulation until the required criteria is reached.

As the number of individuals increases, Fig. 4 demonstrates that the fitness of the individuals improves and the performance of the distribution is barely different from the desired result.

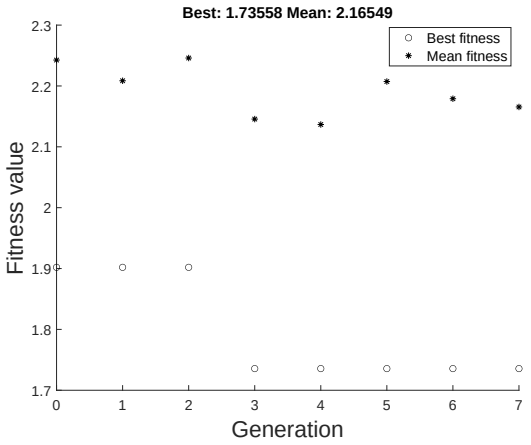

Figure 4: Fitness value of the chosen population size of 18 individuals and 7 generations

The conditions of the run remained the same as for the simulation with the non optimized stirrer geometry. That means that the measurements are taken for 40 stirrer positions and 9 different points spaced out within the chamber. The average value for all points was calculated for both imaginary and real parts in each direction. The distribution of these fields is displayed in Fig.5.

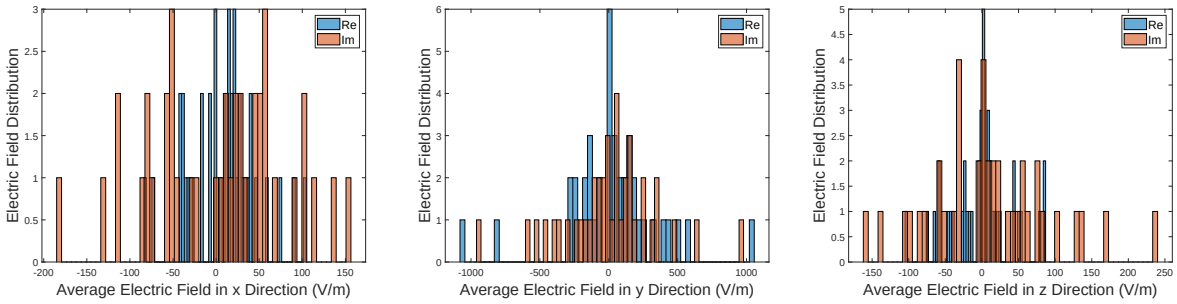

Figure 5: Distribution of the average electric field

The calculation produces the following values for the geometry optimized parameters and P-values for the average electric field distribution.

Table 2: Resulting P-values of the simulation

Symbol	Optimized Values	Unit	Description
tr_1y_1	294	mm	distance
tr_1y_2	28	mm	distance
tr_2y_1	312	mm	distance
tr_2y_2	19	mm	distance

Average Electric Field Distribution	Direction	P-value
Real Part	x	0.4131
	y	0.0019
	z	0.3200
Imaginary Part	x	0.8599
	y	0.1038
	z	0.4860

The P-values from the simulation with the optimized stirrer geometry have improved when compared to the previous simulation but the desired goal has not been reached for all P-values. Therefore, these results lead to the introduction of two more optimized stirrers in remaining x- and y-directions and the optimization of other relevant parameters.

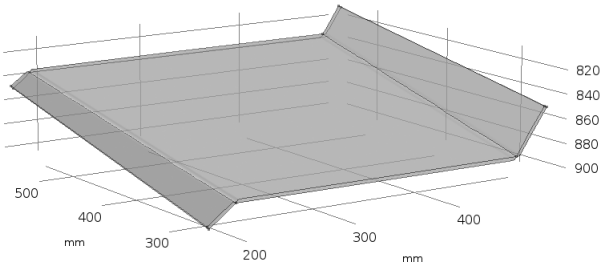

Figure 6: The shape of the optimized stirrer

The Fig. 6 shows the resulting geometry calculated by genetic algorithms.

2.2. Result of the optimized shape for three stirrers

In Fig.7, we observe the reverberation chamber with three stirrer whose geometries have will later be optimized.

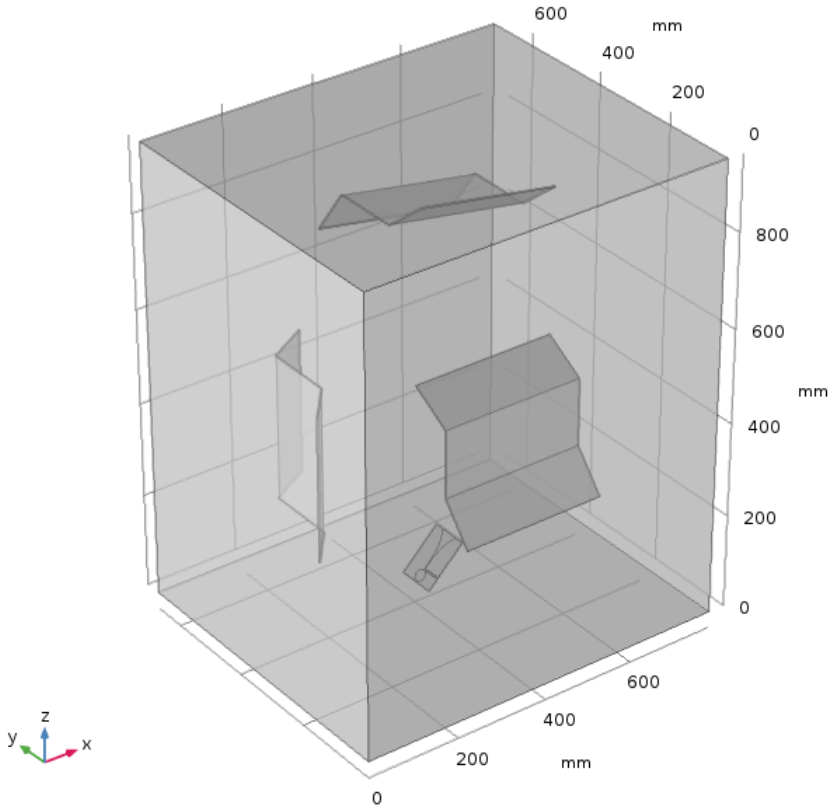

Figure 7: Setup of the resonance chamber with three stirrers, see Table 3 for their postions

The positions of all three stirrers are listed in Table 3.

Table 3: Model parameters and values

Equipment	Parameter	Symbol	Value	Unit
Stirrer 1	Position in x direction	$St_{x,1}$	0	mm
	Position in y direction	$St_{y,1}$	0	mm
	Position in z direction	$St_{z,1}$	860	mm
Stirrer 2	Position in x direction	$St_{x,2}$	0	mm
	Position in y direction	$St_{y,2}$	100	mm
	Position in z direction	$St_{z,2}$	0	mm
Stirrer 3	Position in x direction	$St_{x,3}$	100	mm
	Position in y direction	$St_{y,3}$	0	mm
	Position in z direction	$St_{z,3}$	0	mm

The parameters that have been chosen to be optimized are the shape of the wings for all three stirrers inside the chamber. The newly formulated fitness function for these selected parameters is

$$F_P = \sqrt{\sum_{i=1}^{6} \left| P_i \left(tr_{11}y_1, ..., tr_{23}y_2 \right) - 1 \right|^2} \rightarrow \min. \tag{2}$$

A new solution space for the three stirrers is specified in Table 4.

Table 4: Solution space for genetic algorithms

Equipment	Symbol	Range	Step size	Unit	Description
Stirrer 1	$tr_{11}y_1$	$\begin{bmatrix} 240 & 330 \end{bmatrix}$	9	mm	stirrer wing distance 1
	$tr_{11}y_2$	$\begin{bmatrix} 240 & 330 \end{bmatrix}$	9	mm	stirrer wing distance 2
	$tr_{21}y_1$	$\begin{bmatrix} 10 & 100 \end{bmatrix}$	9	mm	stirrer wing distance 3
	$tr_{21}y_2$	$\begin{bmatrix} 10 & 100 \end{bmatrix}$	9	mm	stirrer wing distance 4
Stirrer 2	$tr_{12}y_1$	$\begin{bmatrix} 240 & 330 \end{bmatrix}$	9	mm	stirrer wing distance 1
	$tr_{12}y_2$	$\begin{bmatrix} 240 & 330 \end{bmatrix}$	9	mm	stirrer wing distance 2
	$tr_{22}y_1$	$\begin{bmatrix} 10 & 100 \end{bmatrix}$	9	mm	stirrer wing distance 3
	$tr_{22}y_2$	$\begin{bmatrix} 10 & 100 \end{bmatrix}$	9	mm	stirrer wing distance 4
Stirrer 3	$tr_{13}y_1$	$\begin{bmatrix} 240 & 330 \end{bmatrix}$	9	mm	stirrer wing distance 1
	$tr_{13}y_2$	$\begin{bmatrix} 240 & 330 \end{bmatrix}$	9	mm	stirrer wing distance 2
	$tr_{23}y_1$	$\begin{bmatrix} 10 & 100 \end{bmatrix}$	9	mm	stirrer wing distance 3
	$tr_{23}y_2$	$\begin{bmatrix} 10 & 100 \end{bmatrix}$	9	mm	stirrer wing distance 4

As previously explained, a population with the chosen size of 18 individuals and 7 generations is generated through the algorithm. Fig. 8 displays the value of the fitness function for each generation.

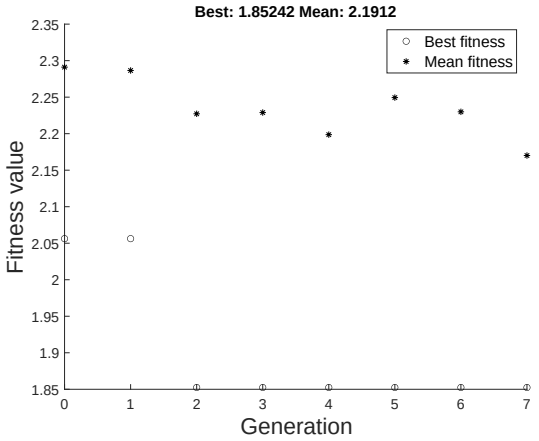

Figure 8: Fitness value of the chosen population size of 18 individuals and 7 generations

The simulation conditions, measurements taken for 40 stirrer positions and 9 different points spaced out within the chamber, remain the same. The histograms on Fig. 9 present the average electric field distribution in all directions for real and imaginary parts.

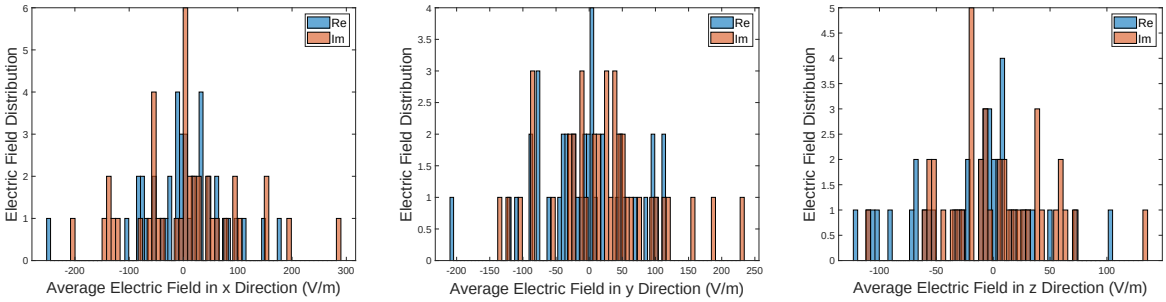

Figure 9: Distribution of the average electric field

Table 5: Resulting P-values of the simulation

Symbol	Optimized Values	Unit
$tr_{11}y_1$	276	mm
$tr_{11}y_2$	240	mm
$tr_{21}y_1$	73	mm
$tr_{21}y_2$	91	mm
$tr_{12}y_1$	276	mm
$tr_{12}y_2$	258	mm
$tr_{22}y_1$	91	mm
$tr_{22}y_2$	28	mm
$tr_{13}y_1$	321	mm
$tr_{13}y_2$	312	mm
$tr_{23}y_1$	64	mm
$tr_{23}y_2$	91	mm

Average Electric Field Distribution	Direction	P-value
Real Part	x	0.0720
	y	0.7291
	z	0.0824
Imaginary Part	x	0.1880
	y	0.4979
	z	0.1378

In conclusion, as seen in Table 5, all resulting P-values have finally fulfilled the desired goal of at least 5% in all directions. This means that, when equiped with three optimised stirrers, the ERC can achieve a normal distribution of the electric field inside the chamber cavity with no further optimizations or changes needed. Of note, is the observation that the optimized stirrers in all cases have favored some symmetrical geometries than initially predicted. This has additionally resulted in stirrers with flater and wider reflective surfaces and smaller stirrer wings.

2.3. Result for using different built-in objects in ERC

Following several simulations and evaluations, the subsequent distributions of the average electric field for both geometries were produced. Fig. 10 represent the electric field distribution for the model with half spheres in all three directions.

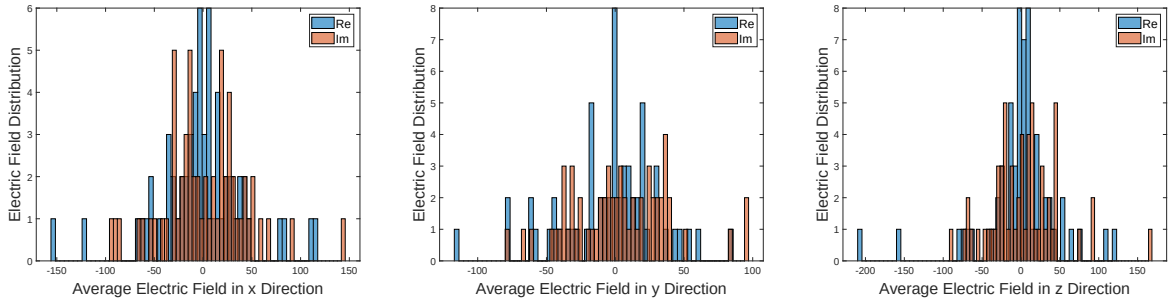

Figure 10: Distribution of the average electric field for half spheres

Subsequently, the electric field distribution for the reverberation chamber with the cones was simulated and represented in Fig. 11. This distribution is, as well, shown for all three directions and for both real and imaginary part. All figures already serve to portray the difference between the two models. At first sight, one can so far determine that the distribution observed for figures relating to the half spheres end up fulfilling expectations more so than those of the cones. These observations are further proven true in Table 6.

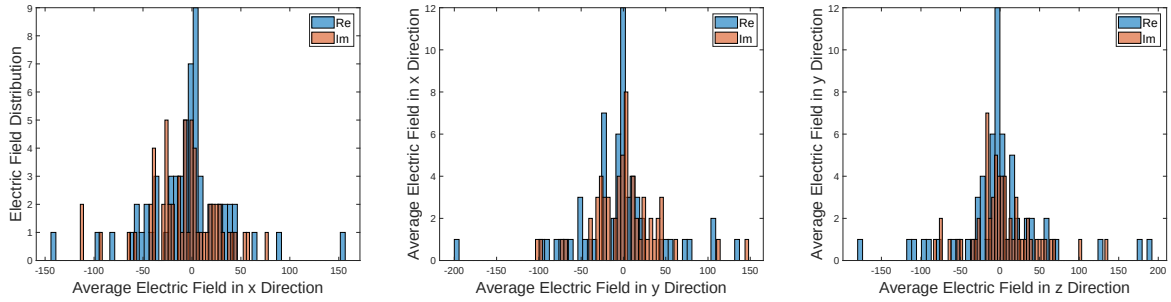

Figure 11: Distribution of the average electric field for cones

The resulting P-values achieved by both models are listed below in Table 6 and given for both real and imaginary parts of the field.

Table 6: Resulting P-values of the simulation

Average Electric Field Distribution	Direction	P-value of Half Sphere	P-value of Cone
Real Part	x	0.0024	3.4875×10^{-4}
	y	0.0513	2.6074×10^{-4}
	z	6.2473×10^{-6}	2.7340×10^{-5}
Imaginary Part	x	0.0893	0.0294
	y	0.2413	9.0150×10^{-4}
	z	0.0095	0.0085

The P-values serve to emphasize the contrast of both geometries and, thus, help in the choice of a better suited geometry for the ERC. The P-values calculated for the half spheres are remarkably better than those of the cones as half of them succeed the previously established desired goal of at least 5%, whereas none of the values of the cone simulation come even close to approaching the needed standard. Nevertheless, the P-values are still not perfect and need to be optimized further.

3. Technical implementation

The GA are implemented in Matlab and thus the initial population is created. The values of the parameters are transmitted to Comsol via Livelink, an interface between Matlab and Comsol. With these values, Comsol simulates the model of the fuel cell and determines the cell current for dierent voltages using finite element method. Matlab get the data through Livelink and calculate the power curve. This is compared with the indicated desired power curve and new values for the parameters are calculated through GA. Finally, the parameters are transmitted to Comsol again and the loop runs until the termination criteria are reached.

The calculation time of the implementation is:

$$T_{imp} = n_I * n_G * T_{sim} \tag{3}$$

where n_P is the number of individuals, n_G the number of generations and T_{sim} the time for each simulation. In the mentioned case, the size of the simulation included 8 individuals and 7 generations. A computer with the power of 2.8 GHz CPU and 32 GB RAM was used. For the simulation for fuel cell each simulation lasted in 1 minute and 45 seconds. The total calculation time yielded about 2 hours. The opimization simulation of the optimized stirrer geometry and the performance to optimized the shape of three stirrer yielded about 70 hours. The size of the simulation included 18 individuals and 7 generations.